Supplementary Information for

Formation drivers and photochemical effects of $ClNO_2$ in a coastal city of Southeast China

Gaojie Chen[1,4,5], Xiaolong Fan[1,4], Haichao Wang[2*], Yee Jun Tham[3], Ziyi Lin[1,4,5], Xiaoting Ji[1,4,5], Lingling Xu[1,4], Baoye Hu[6], Jinsheng Chen[1,4*]

[1]Center for Excellence in Regional Atmospheric Environment, Institute of Urban Environment, Chinese Academy of Sciences, Xiamen 361021, China

[2]School of Atmospheric Sciences, Sun Yat-sen University, Zhuhai 519082, China

[3]School of Marine Sciences, Sun Yat-sen University, Zhuhai 519082, China

[4]Fujian Key Laboratory of Atmospheric Ozone Pollution Prevention, Institute of Urban Environment, Chinese Academy of Sciences, Xiamen 361021, China

[5]University of Chinese Academy of Sciences, Beijing 100049, China

[6]Minnan Normal University, Zhangzhou 363000, China

*Correspondence to: Jinsheng Chen (jschen@iue.ac.cn); Haichao Wang (wanghch27@mail.sysu.edu.cn).

Captions:

Text S1. Detailed information of this observation site and instruments.

Text S2. The calibrations of $ClNO_2$ and N_2O_5 and uncertainty analysis.

Text S3. The model configuration of machine learning.

Text S4. The box model configuration.

Fig. S1 Measurement locations. (a) Location of Xiamen City in the southeast of China. (b) Location of the measurement site in Xiamen.

Fig. S2 The dependences of $ClNO_2$ and N_2O_5 sensitivity on relative humidity.

Fig. S3 Comparison of observed $ClNO_2$ concentrations and simulated concentrations of $ClNO_2$ by the XGBoost model.

Fig. S4 RO_x ($OH + HO_2 + RO_2$) radicals production rates induced by $ClNO_2$ photolysis under the observation-average conditions and the high $ClNO_2$ case.

Fig. S5 Increased percentages of RO_x (OH, HO_2, RO_2) radicals induced by $ClNO_2$ photolysis under the observation-average and case conditions.

Table S1. Measurement techniques, time resolutions, and detection limit of observation instruments at our study site.

Table S2. The observation data used in the box model under the observation-average conditions and the high $ClNO_2$ case (Unit: ppb).

Table S3. Summary of $ClNO_2$ peak concentrations at different types of sites in China and other countries (Unit: ppb).

Text S1. Detailed information of this observation site and instruments.

The observation site is on the top of the teaching building (over 70 meters) of Institute of Urban Environment, Chinese Academy of Sciences in Xiamen, surrounded by school and residential buildings, Xinglin Bay, and several major transportation roads (Fig.S1). The observation site, called as the Atmospheric Observation Supersite, is equipped with complete measurement instruments to observe trace gases, aerosol compositions, and meteorological parameters. The continuous gas analyzers (Thermo Fisher Scientific, USA) were employed to measure O_3 (TEI 49*i*), CO (TEI 48*i*), SO_2 (TEI 43*i*), and NO_x (TEI 42*i*). VOC species were detected by a gas chromatography system equipped with a mass spectrometer and flame ionization detector (GC-MS/FID, TH-300B, Wuhan, China). $PM_{2.5}$ mass concentrations and its inorganic compositions (NO_3^-, SO_4^{2-}, NH_4^+, and Cl^-) were monitored using the tapered element oscillating microbalance (TEOM1405, Thermo Scientific Corp., MA, USA) and the Monitor for AeRosols and Gases in ambient Air (MARGA; ADI 2080, Applikon Analytical B.V., the Netherlands), respectively. The particle surface area concentrations (*S*a) were obtained from the ambient particle number size distribution detecting by the Scanning Mobility Particle Sizer (SMPS, TSI Inc.) and Aerodynamic Particle Size Spectrometer (APS). Meteorological factors, including air temperature (T), relative humidity (RH), atmospheric pressure (P), ultraviolet radiation (UV), wind speed (WS), and wind direction (WD) were measured by the weather station with a sonic anemometer (150WX, Airmar, USA). The data of boundary layer height (BLH) was gotten from the European Centre for Medium-Range Weather Forecasts (ECMWF) ERA5 hourly reanalysis dataset. Photolysis frequency (including $J(O^1D)$, $J(NO_2)$, J(HCHO), J(HONO), $J(NO_3)$, and $J(H_2O_2)$) were detected by a photolysis spectrometer (PFS-100, Focused Photonics Inc., Hangzhou, China). The HCHO analyzer (FMS-100, Focused Photonics Inc., Hangzhou, China) was used to observe the concentrations of HCHO.

The concentrations of $ClNO_2$ and N_2O_5 were measured by an iodide-adduct Chemical Ionization-Atmospheric Pressure Interface-Long Time of Flight (Aerodyne Research Inc, USA and Tofwerk AG, Switzerland) mass spectrometer (I^--ToF-CIMS). The ambient air is drawn into the sampling chamber through a perfluoroalkoxy (PFA) pipeline, approximately 2 meters in length with an inner diameter of 1/4 inch, at a flow rate of 10 standard liters per minute (SLPM). Subsamples of approximately 2 SLPM are then introduced into the CIMS setting. Within this setup, methyl iodine gas (CH_3I) emitted from the heated CH_3I permeation tube (VICI) undergoes ionization as it passes through a soft X-ray ionization source (Tofwerk AG, P-type), carried by an ultra-high purity nitrogen gas (N_2) flow at 99.999% purity and a rate of 2.7 SLPM. Reagent ions (I^- and $I(H_2O)^-$) selectively participate in the ion-molecule reaction (IMR) chamber with the target gas,

producing iodide clusters in the IMR chamber. These clusters are then quantified using the I^--ToF-CIMS instrument. The background signals of the CIMS instrument were determined by introducing dry N_2 into the inlet for a duration of 20 minutes. To prevent the buildup of particulate matter on the inlet tubing, we replaced the tubing weekly and flushed it with deionized water, followed by a 20-minute stream of N_2 for drying. Additionally, to reduce interference from the sampling inlet, we utilized a pump with a flow rate of 10 SLPM to draw the ambient sample.

Text S2. The calibrations of $ClNO_2$ and N_2O_5 and uncertainty analysis.

In our study, the calibrations of $ClNO_2$ and N_2O_5 were based on previous established methods (Thaler et al., 2011; Wang et al., 2016; Wang et al., 2022). A nitrogen (N_2) flow at a rate of 50 $mL \cdot min^{-1}$, containing 6 ppm of Cl_2, was directed over a slurry composed of sodium nitrite ($NaNO_2$) and sodium chloride (NaCl). This slurry facilitated the production of $ClNO_2$, with NaCl added to minimize NO_2 formation as a secondary product. Subsequently, the resulting mixture containing $ClNO_2$ was conditioned to a specified RH and then sampled using the CIMS instrument. To quantify the concentrations of $ClNO_2$, the mixed flow was directly fed into a cavity attenuated phase shift spectroscopy (CAPS) instrument to measure the baseline levels of NO_2, subsequently, it was passed through a thermal dissociation tube heated to 380 ℃, causing $ClNO_2$ to decompose into NO_2, determined by the CAPS instrument. The differences in measured NO_2 concentrations between with and without thermal dissociation corresponded to the concentrations of $ClNO_2$. For the calibration of N_2O_5, O_3 was generated by passing approximately 30 sccm of ultrapure zero air through a mercury lamp (UVP). O_3 then reacted with a 30 sccm flow rate of NO_2 to produce NO_3, which subsequently reacted with NO_2 to yield a flow of N_2O_5. This N_2O_5-enriched flow was utilized to calibrate the CIMS measurements of N_2O_5. By adjusting the RH, a mixed flow containing stable N_2O_5 was introduced into the CIMS instrument, allowing for the acquisition of a normalized humidity-dependent curve for N_2O_5. Although the absolute concentrations of the N_2O_5 source were not directly quantified due to the absence of an N_2O_5-specific detector, the N_2O_5-enriched flow was passed through a supersaturated NaCl solution assuming 100% conversion efficiency from N_2O_5 to $ClNO_2$. The dependences of CNO_2 and N_2O_5 sensitivity on RH are shown in Fig. S2, indicating that the sensitivities of $ClNO_2$ and N_2O_5 depended on the variations of RH values. The sensitivities of $ClNO_2$ and N_2O_5 were 0.055 ± 0.018 and 0.11 ± 0.063 $ncps \cdot ppb^{-1}$, respectively. The detection limit (3σ) of $ClNO_2$ and N_2O_5 was 1.3 and 0.61 ppt, respectively.

Text S3. The model configuration of machine learning.

The gradient boosted tree implemented from XGBoost was chosen as machine learning methods. It has been optimized to run in distributed computing environment and can handle a large amount of input data. Compared to neural networks, the results of gradient boosting tree models are more interpretable, enabling them to link the results with the recognizable chemical features. The XGBoost algorithm is a tree-based machine learning model known for its excellent performance in speed and accuracy. It can aggregate weak learners into a strong model, enhancing single generalization ability and robustness, thereby improving prediction accuracy.

In this study, $ClNO_2$ concentrations are as dependent variable, and trace gases (SO_2, CO, NO_2, NO, O_3, and N_2O_5), $PM_{2.5}$, inorganic compositions (NO_3^-, SO_4^{2-}, NH_4^+, and Cl^-), and meteorological parameters (T, RH, UV, WS, WD, and BLH) are as the argument. In the XGBoost model, 70% of the observed data are used as the training set, and the rest 30% data are used as the testing set. Five cross-validation is employed to adjust hyperparameters to stabilize the predictive ability of the model. The adjusted hyperparameters include maximum depth, learning rate, gamma, minimum child weight, and estimate. R^2, mean square error (MSE), and root mean square error (RMSE) are used to assess the model performance. The Shapely additive explanations (SHAP) model is an interpreter package designed to investigate the contributions of each feature to the model predictions. Its approach involves an additive explanatory model which treats all features as contributors, a concept inspired by cooperative game theory. For each predicted sample, the SHAP model provides a Shapley value, which is the sum of the values assigned to each feature.

Text S4. The box model configuration and output.

The observation-based model (OBM) coupled with the Master Chemical Mechanism (MCM) version 3.3.1 was utilized to assess the impacts of $ClNO_2$ on photochemically atmospheric oxidation. As delineated in earlier studies (Xue et al., 2015; Tham et al., 2016; Xia et al., 2021; Peng et al., 2021; Peng et al., 2022), established chlorine chemistry mechanisms have been integrated. The impacts of dilution mixing were included for all species by introducing a dilution factor, defined as a function of the variation of the planetary boundary layer (PBL) height. In our study, $ClNO_2$, N_2O_5, VOCs, HCHO, HONO, CO, O_3, NO, NO_2, SO_2, along with meteorological factors as observation constrained were input into the box model at an hourly resolution. We performed the OBM for 5 days to initialize the unconstrained compounds and radicals before starting the simulation. We focused on elucidating the influence of $ClNO_2$ photolysis on the formation of RO_x radicals and O_3, the AOC. Generally, the reactions of HO_2 + NO and RO_2 + NO are the major O_3 production

pathways (Eq.1), and the O_3 loss pathways (Eq.2) include NO_2 + OH/RO_2, O_3 photolysis, O_3 + OH/HO_2 radicals, O_3/NO_3+ VOCs. The O_3 production rate minus the O_3 loss rate was used to calculate the net O_3 production rate (Eq.3).

$$P(O_3) = k_1[HO_2][NO] + \sum(k_2[RO_2][NO]) \quad (1)$$

$$L(O_3) = k_3[O_1D][H_2O] + k_4[O_3][OH] + k_5[O_3][HO_2] + k_6[NO_2][OH] + \sum(k_7[O_3][VOCs]) + 2\sum(k_8[NO_3][VOCs]) \quad (2)$$

$$P_{net}(O_3) = P(O_3) - L(O_3) \quad (3)$$

Where, k_i stands for the rate constant.

The AOC is calculated by the sum of the rates of CH_4, CO, and VOCs oxidized by atmospheric oxidants (O_3, OH, Cl, and NO_3 radicals) (Xue et al., 2015; Yi et al., 2023), used by Eq. (4).

$$AOC = \sum_i k_{Y_i}[Y_i][X] \quad (4)$$

Where, $[Y_i]$ is the concentrations of reduced species (VOCs, CO, and CH_4), $[X]$ is the concentrations of oxidants (O_3, OH, Cl, and NO_3 radicals), and k_{Yi} represents the reaction rate constant of Y_i and X.

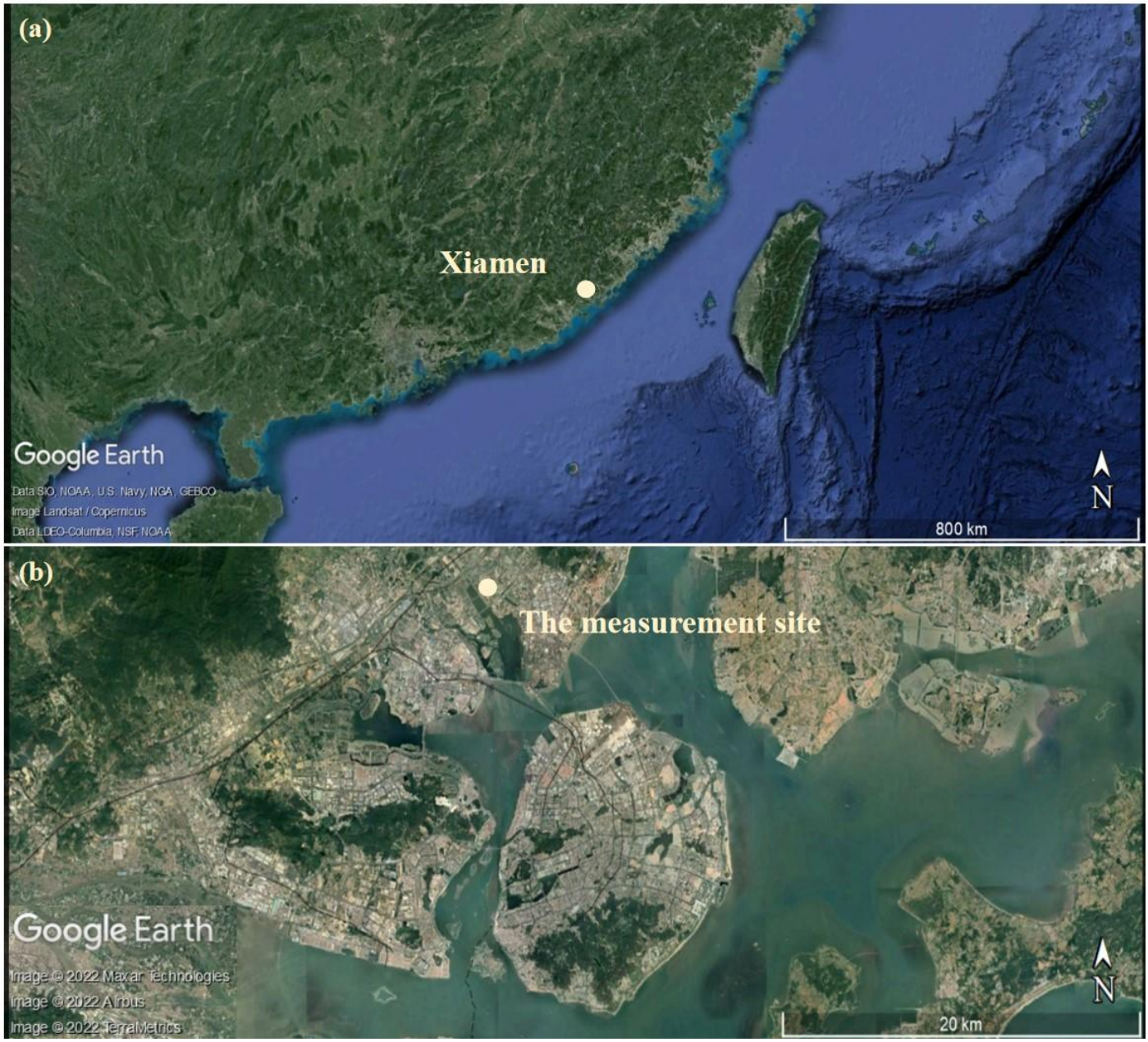

Fig. S1 Measurement locations. (a) Xiamen City in the southeast of China. (b) Location of the measurement site in Xiamen. (The topographic image is provided by © Google Earth.)

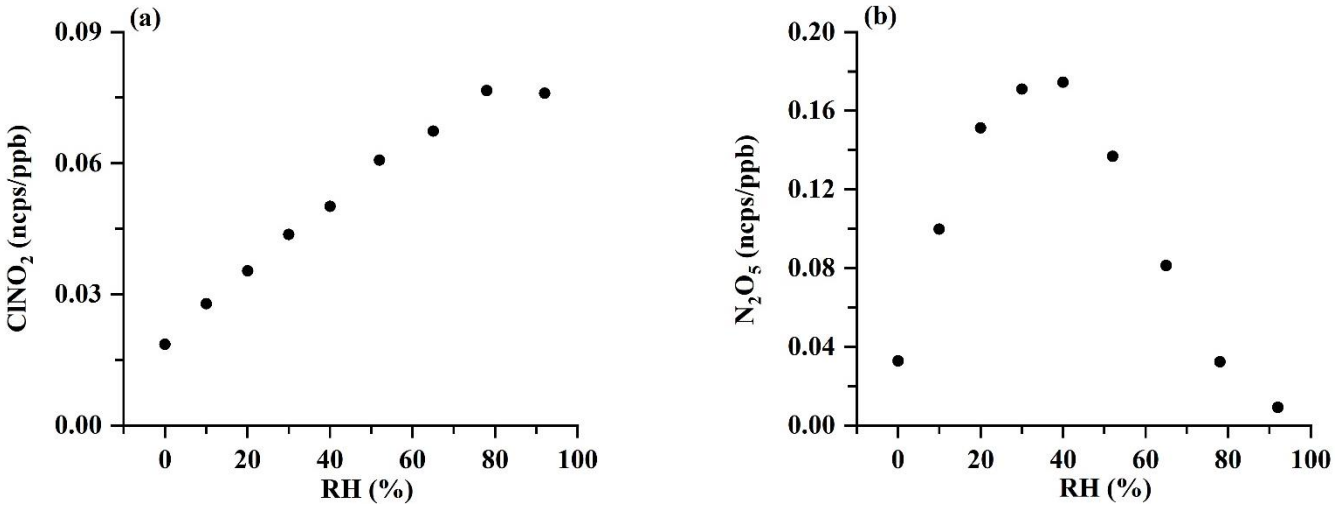

Fig. S2 The dependences of $ClNO_2$ and N_2O_5 sensitivity on relative humidity.

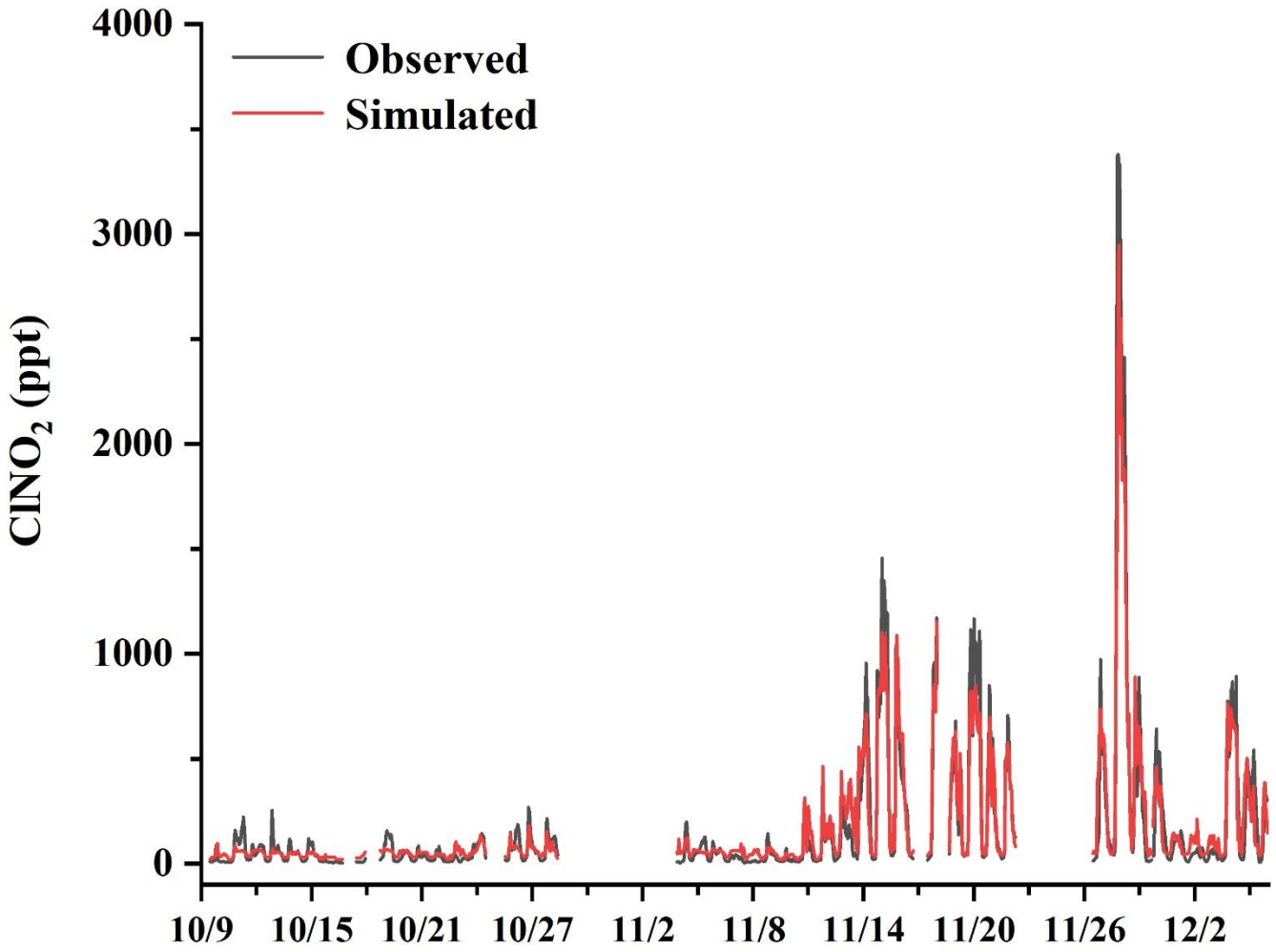

Fig. S3 Comparison of observed $ClNO_2$ concentrations and simulated concentrations of $ClNO_2$ by the XGBoost model.

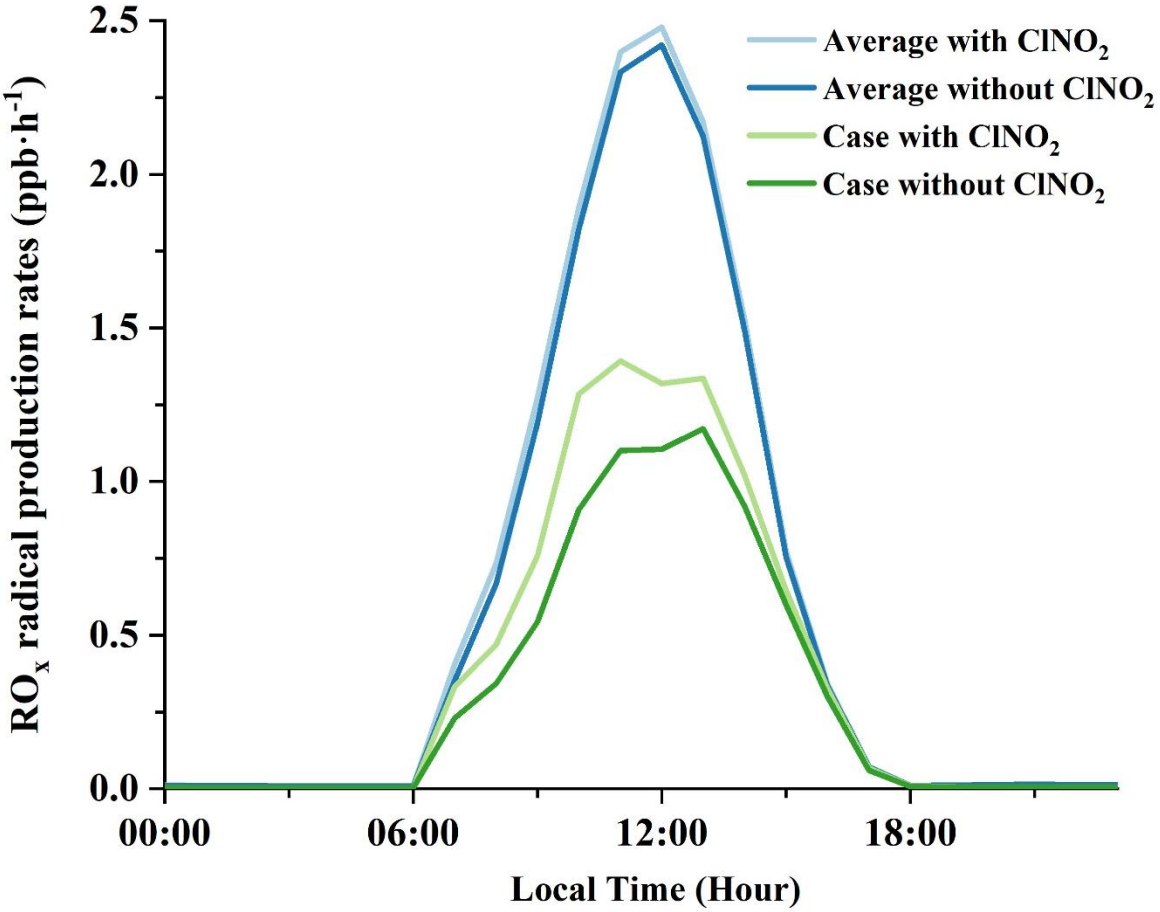

200

201 **Fig. S4** RO_x ($OH + HO_2 + RO_2$) radicals production rates induced by $ClNO_2$ photolysis under the observation-

202 average conditions and the high $ClNO_2$ case.

203

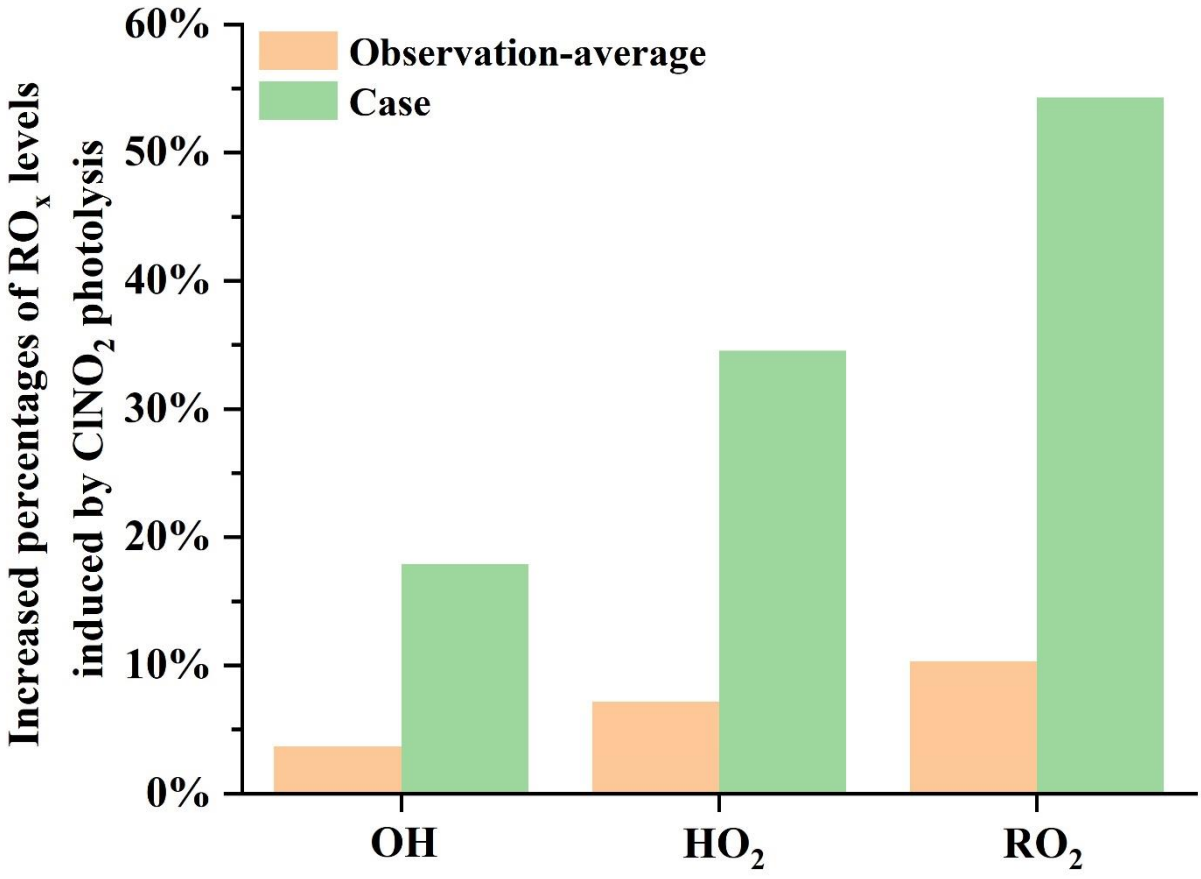

Fig. S5 Increased percentages of RO_x (OH, HO_2, RO_2) radicals induced by $ClNO_2$ photolysis under the observation-average conditions and the high $ClNO_2$ case.

Table S1. Measurement techniques, time resolutions, and detection limit of observation instruments at our study site.

Parameters	Techniques	Time resolutions	Limit of detection
$ClNO_2$ and N_2O_5	I^--ToF-CIMS	1 min	~ 1 ppt
CH_4	NCMS6300	15 min	21 ppb
VOCs	GC-MS/FID	1 hour	0.02-0.30 ppb
HCHO	Hantzsch fluorimetry	1 s	0.05 ppb
$J(O^1D)$, $J(NO_2)$, J(HONO), $J(NO_3)$, J(HCHO), and $J(H_2O_2)$	Photolysis spectrometer	8 s	a
CO	Infrared absorption	1 min	40.00 ppb
SO_2	Pulsed UV fluorescence	1 min	0.50 ppb
O_3	UV photometry	1 min	1.00 ppb
NO	Chemiluminescence	1 min	0.50 ppb
NO_2	Chemiluminescence	1 min	0.50 ppb

a. Process-specific, 5 orders of magnitude lower than maximum at noon.

Table S2. The observation data used in the box model under the observation-average conditions and the high $ClNO_2$ case (Unit: ppb).

Parameters	Average	Case	Parameters	Average	Case
T (K)	296.77	295.63	M2HEX	0.04	0.04
RH (%)	65.98	88.48	M3HEX	0.06	0.08
SO_2	1.93	2.34	NC7H16	0.06	0.06
NO_2	12.94	26.38	TOLUENE	1.12	1.73
NO	3.19	5.85	NC8H18	0.02	0.02
CO	461.59	769.56	PXYL	0.40	0.73
O_3	31.07	11.43	EBENZ	0.19	0.42
C2H4	0.89	1.41	NC9H20	0.01	0.02
C2H2	0.78	1.53	STYRENE	0.04	0.09
C2H6	2.01	2.64	OXYL	0.11	0.20
C3H6	0.24	0.23	TM124B	0.02	0.03
C3H8	1.90	3.28	TM123B	0.01	0.01
IC4H10	0.74	1.30	NC11H24	0.01	0.01
BUT1ENE	0.05	0.06	NC12H26	0.02	0.03
NC4H10	1.07	1.97	HCHO	2.50	3.92
CBUT2ENE	0.02	0.03	ACR	0.06	0.06
TBUT2ENE	0.02	0.03	CH3COCH3	1.98	2.26
IC5H12	0.61	1.46	MEK	0.47	0.52
NC5H12	0.27	0.50	CH3CL	0.39	0.33
C5H8	0.02	0.02	C4H6	0.01	0.02
M22C4	0.02	0.02	IPROPOL	0.17	0.11
M23C4	0.05	0.06	MTBE	0.10	0.19
M2PE	0.05	0.08	ETHACET	1.26	2.14
M3PE	0.08	0.13	$J NO_2$ (s^{-1})	0.002106	0.000981
HEX1ENE	0.00	0.00	$ClNO_2$	0.17	0.96
NC6H14	0.09	0.15	N_2O_5	0.02	0.01
BENZENE	0.18	0.32	Cl_2	0.01	0.05
CHEX	0.02	0.02	HONO	0.48	0.77

Table S3. Summary of $ClNO_2$ peak concentrations at different types of sites in China and other countries (Unit: ppb).

Observation Area	Observation Sites	$ClNO_2$	References
Wangdu, China	Rural site	~3.5	1
Beijing, China	Urban site	~3.0	2
Jinan, China	Urban site	~0.8	3
Mt. Tai, China	Mountain site	~2.0	4
Changzhou, China	Suburban site	~1.3	5
Shanghai, China	Urban site	~5.7	5
Nanjing, China	Rural site	~3.7	6
Xiamen, China	Urban site	~3.4	This study
Heshan, China	Rural site	~8.1	7
Shenzhen, China	Background site	~1.7	8
Hong Kong, China	Mountain site	~4.7	9
Seoul, Korea	Urban site	~2.5	10
Hesen, Germany	Rural site	~0.8	11
London, UK	Urban site	~0.7	12
Boulder, USA	Urban site	~1.3	13
Houston, USA	Marine boundary layer	~1.2	14
Los Angeles, USA	Marine boundary layer	~3.5	15
Calgary, Canada	Urban site	~0.3	16

The references as follows:1 (Tham et al., 2016), 2 (Ma et al., 2023), 3 (Wang et al., 2017a), 4 (Wang et al., 2017b), 5 (Li et al., 2023), 6 (Xia et al., 2020), 7 (Yun et al., 2018), 8 (Niu et al., 2022), 9 (Wang et al., 2016), 10 (Jeong et al., 2019), 11 (Phillips et al., 2012), 12 (Bannan et al., 2015), 13 (Thornton et al., 2010), 14 (Osthoff et al., 2008), 15 (Riedel et al., 2012), 16 (Mielke et al., 2011).

References

Bannan, T. J., Booth, A. M., Bacak, A., Muller, J. B. A., Leather, K. E., Le Breton, M., Jones, B., Young, D., Coe, H., Allan, J., Visser, S., Slowik, J. G., Furger, M., Prévôt, A. S. H., Lee, J., Dunmore, R. E., Hopkins, J. R., Hamilton, J. F., Lewis, A. C., Whalley, L. K., Sharp, T., Stone, D., Heard, D. E., Fleming, Z. L., Leigh, R., Shallcross, D. E., and Percival, C. J.: The first UK measurements of nitryl chloride using a chemical ionization mass spectrometer in central London in the summer of 2012, and an investigation of the role of Cl atom oxidation, J. Geophys. Res. Atmos., 120, 5638-5657, https://doi.org/10.1002/2014jd022629, 2015.

Jeong, D., Seco, R., Gu, D., Lee, Y., Nault, B. A., Knote, C. J., McGee, T., Sullivan, J. T., Jimenez, J. L., Campuzano-Jost, P., Blake, D. R., Sanchez, D., Guenther, A. B., Tanner, D., Huey, L. G., Long, R., Anderson, B. E., Hall, S. R., Ullmann, K., Shin, H., Herndon, S. C., Lee, Y., Kim, D., Ahn, J., and Kim, S.: Integration of airborne and ground observations of nitryl chloride in the Seoul metropolitan area and the implications on regional oxidation capacity during KORUS-AQ 2016, Atmos. Chem. Phys., 19, 12779-12795, https://doi.org/10.5194/acp-19-12779-2019, 2019.

Li, F., Huang, D. D., Nie, W., Tham, Y. J., Lou, S., Li, Y., Tian, L., Liu, Y., Zhou, M., and Wang, H. J. A. E.: Observation of nitrogen oxide-influenced chlorine chemistry and source analysis of Cl_2 in the Yangtze River Delta, China, Atmos. Environ., 306, 119829, https://doi.org/10.1016/j.atmosenv.2023.119829, 2023.

Ma, W., Chen, X., Xia, M., Liu, Y., Wang, Y., Zhang, Y., Zheng, F., Zhan, J., Hua, C., Wang, Z. J. E. S., and Technology: Reactive Chlorine Species Advancing the Atmospheric Oxidation Capacities of Inland Urban Environments, Environ. Sci. Technol., 57, 14638-14647, https://doi.org/10.1021/acs.est.3c05169, 2023.

Mielke, L. H., Furgeson, A., and Osthoff, H. D.: Observation of $ClNO_2$ in a Mid-Continental Urban Environment, Environ. Sci. Technol., 45, 8889-8896, https://doi.org/10.1021/es201955u, 2011.

Niu, Y.-B., Zhu, B., He, L.-Y., Wang, Z., Lin, X.-Y., Tang, M.-X., and Huang, X.-F.: Fast Nocturnal Heterogeneous Chemistry in a Coastal Background Atmosphere and Its Implications for Daytime Photochemistry, J. Geophys. Res. Atmos., 127, e2022JD036716, https://doi.org/10.1029/2022JD036716, 2022.

Osthoff, H. D., Roberts, J. M., Ravishankara, A. R., Williams, E. J., Lerner, B. M., Sommariva, R., Bates, T. S., Coffman, D., Quinn, P. K., Dibb, J. E., Stark, H., Burkholder, J. B., Talukdar, R. K., Meagher, J., Fehsenfeld,

F. C., and Brown, S. S.: High levels of nitryl chloride in the polluted subtropical marine boundary layer, Nat. Geosci., 1, 324-328, https://doi.org/10.1038/ngeo177, 2008.

Peng, X., Wang, T., Wang, W., Ravishankara, A., George, C., Xia, M., Cai, M., Li, Q., Salvador, C. M., and Lau, C. J. N. c.: Photodissociation of particulate nitrate as a source of daytime tropospheric Cl_2, Nat. Commun., 13, 1-10, https://doi.org/10.1038/s41467-022-28383-9, 2022.

Peng, X., Wang, W., Xia, M., Chen, H., Ravishankara, A. R., Li, Q., Saiz-Lopez, A., Liu, P., Zhang, F., Zhang, C., Xue, L., Wang, X., George, C., Wang, J., Mu, Y., Chen, J., and Wang, T.: An unexpected large continental source of reactive bromine and chlorine with significant impact on wintertime air quality, Natl. Sci. Rev., 8, nwaa304, https://doi.org/10.1093/nsr/nwaa304, 2021.

Phillips, G. J., Tang, M. J., Thieser, J., Brickwedde, B., Schuster, G., Bohn, B., Lelieveld, J., and Crowley, J. N.: Significant concentrations of nitryl chloride observed in rural continental Europe associated with the influence of sea salt chloride and anthropogenic emissions, Geophys. Res. Lett., 39, L10811, https://doi.org/10.1029/2012gl051912, 2012.

Riedel, T. P., Bertram, T. H., Crisp, T. A., Williams, E. J., Lerner, B. M., Vlasenko, A., Li, S. M., Gilman, J., de Gouw, J., Bon, D. M., Wagner, N. L., Brown, S. S., and Thornton, J. A.: Nitryl chloride and molecular chlorine in the coastal marine boundary layer, Environ. Sci. Technol., 46, 10463-10470, https://doi.org/10.1021/es204632r, 2012.

Thaler, R. D., Mielke, L. H., and Osthoff, H. D.: Quantification of nitryl chloride at part per trillion mixing ratios by thermal dissociation cavity ring-down spectroscopy, Anal. Chem., 83, 2761-2766, https://doi.org/10.1021/ac200055z, 2011.

Tham, Y. J., Wang, Z., Li, Q., Yun, H., Wang, W., Wang, X., Xue, L., Lu, K., Ma, N., Bohn, B., Li, X., Kecorius, S., Größ, J., Shao, M., Wiedensohler, A., Zhang, Y., and Wang, T.: Significant concentrations of nitryl chloride sustained in the morning: investigations of the causes and impacts on ozone production in a polluted region of northern China, Atmos. Chem. Phys., 16, 14959-14977, https://doi.org/10.5194/acp-16-14959-2016, 2016.

Thornton, J. A., Kercher, J. P., Riedel, T. P., Wagner, N. L., Cozic, J., Holloway, J. S., Dubé, W. P., Wolfe, G. M., Quinn, P. K., Middlebrook, A. M., Alexander, B., and Brown, S. S.: A large atomic chlorine source inferred from mid-continental reactive nitrogen chemistry, Nature., 464, 271-274, https://doi.org/10.1038/nature08905,

2010.

Wang, H., Yuan, B., Zheng, E., Zhang, X., Wang, J., Lu, K., Ye, C., Yang, L., Huang, S., Hu, W. J. A. C., and Physics: Formation and impacts of nitryl chloride in Pearl River Delta, Atmos. Chem. Phys., 22, 14837-14858, https://doi.org/10.5194/acp-22-14837-2022, 2022.

Wang, T., Tham, Y. J., Xue, L., Li, Q., Zha, Q., Wang, Z., Poon, S. C. N., Dubé, W. P., Blake, D. R., Louie, P. K. K., Luk, C. W. Y., Tsui, W., and Brown, S. S.: Observations of nitryl chloride and modeling its source and effect on ozone in the planetary boundary layer of southern China, J. Geophys. Res. Atmos., 121, 2476-2489, https://doi.org/10.1002/2015JD024556, 2016.

Wang, X., Wang, H., Xue, L., Wang, T., Wang, L., Gu, R., Wang, W., Tham, Y. J., Wang, Z., and Yang, L. J. A. e.: Observations of N_2O_5 and $ClNO_2$ at a polluted urban surface site in North China: High N_2O_5 uptake coefficients and low $ClNO_2$ product yields, Atmos. Environ., 156, 125-134, http://dx.doi.org/10.1016/j.atmosenv.2017.02.035, 2017a.

Wang, Z., Wang, W., Tham, Y. J., Li, Q., Wang, H., Wen, L., Wang, X., and Wang, T.: Fast heterogeneous N_2O_5 uptake and $ClNO_2$ production in power plant and industrial plumes observed in the nocturnal residual layer over the North China Plain, Atmos. Chem. Phys., 17, 12361-12378, https://doi.org/10.5194/acp-17-12361-2017, 2017b.

Xia, M., Peng, X., Wang, W., Yu, C., Wang, Z., Tham, Y. J., Chen, J., Chen, H., Mu, Y., Zhang, C. J. A. C., and Physics: Winter $ClNO_2$ formation in the region of fresh anthropogenic emissions: seasonal variability and insights into daytime peaks in northern China, Atmos. Chem. Phys., 21, 15985-16000, https://doi.org/10.5194/acp-21-15985-2021, 2021.

Xia, M., Peng, X., Wang, W., Yu, C., Sun, P., Li, Y., Liu, Y. A. H. C. t. A.-P. O. A. C., Xu, Z., Wang, Z., Xu, Z., Nie, W., Ding, A., and Wang, T.: Significant production of $ClNO_2$ and possible source of Cl_2 from N_2O_5 uptake at a suburban site in eastern China, Atmos. Chem. Phys., 20, 6147-6158, https://doi.org/10.5194/acp-20-6147-2020, 2020.

Xue, L. K., Saunders, S. M., Wang, T., Gao, R., Wang, X. F., Zhang, Q. Z., and Wang, W. X.: Development of a chlorine chemistry module for the Master Chemical Mechanism, Geosci. Model Dev., 8, 3151-3162, https://doi.org/10.5194/gmd-8-3151-2015, 2015.

Yi, X., Sarwar, G., Bian, J., Huang, L., Li, Q., Jiang, S., Liu, H., Wang, Y., Chen, H., and Wang, T. J. J. o. G. R. A.: Significant Impact of Reactive Chlorine on Complex Air Pollution Over the Yangtze River Delta Region, China, J. Geophys. Res. Atmos., 128, e2023JD038898, https://doi.org/10.1029/2023JD038898, 2023.

Yun, H., Wang, T., Wang, W., Tham, Y. J., Li, Q., Wang, Z., and Poon, S. C. N.: Nighttime NO_x loss and $ClNO_2$ formation in the residual layer of a polluted region: Insights from field measurements and an iterative box model, Sci. Total Environ., 622-623, 727-734, https://doi.org/10.1016/j.scitotenv.2017.11.352, 2018.